HHS Public Access

Author manuscript

Mol Cancer Ther. Author manuscript; available in PMC 2017 April 01.

Published in final edited form as:

Mol Cancer Ther. 2016 April ; 15(4): 608–617. doi:10.1158/1535-7163.MCT-15-0719.

An HRE-binding Py-Im polyamide impairs hypoxic signaling in tumors

Jerzy O. Szablowski[1], **Jevgenij A. Raskatov**[1,*], and **Peter B. Dervan**[a,1]

[1]Division of Chemistry and Chemical Engineering, California Institute of Technology, Pasadena, CA 91125

Abstract

Hypoxic gene expression contributes to the pathogenesis of many diseases, including organ fibrosis, age-related macular degeneration and cancer. HIF-1, a transcription factor central to the hypoxic gene expression, mediates multiple processes including neovascularization, cancer metastasis and cell survival. Py-Im polyamide 1 has been shown to inhibit HIF-1-mediated gene expression in cell culture but its activity *in vivo* was unknown. This study reports activity of polyamide 1 in subcutaneous tumors capable of mounting a hypoxic response and showing neovascularization. We show that 1 distributes into subcutaneous tumor xenografts and normal tissues, reduces the expression of proangiogenic and prometastatic factors, inhibits the formation of new tumor blood vessels and suppresses tumor growth. Tumors treated with 1 show no increase in HIF-1a and have reduced ability to adapt to the hypoxic conditions, as evidenced by increased apoptosis in HIF-1a positive regions and the increased proximity of necrotic regions to vasculature. Overall, these results show that a molecule designed to block the transcriptional activity of HIF-1 has potent anti-tumor activity *in vivo*, consistent with partial inhibition of the tumor hypoxic response.

Keywords

hypoxic signaling; angiogenesis; Py-Im polyamide; phenotypic mechanism; gene expression

Introduction

Oxygen sensing is involved in a range of natural physiological processes such as embryonal development, wound healing and immune response (1). However, its dysregulation can contribute to pathogenesis of multiple diseases including fibrosis, erythrocythemia, heart disease and cancer - a group of diseases leading to nearly 600,000 deaths every year, in the United States alone (2). While new cancer treatments are being developed, many of the cancer therapies are hampered by presence of low levels of oxygen in tumors (3), known as tumor hypoxia, regulated mainly by Hypoxia Inducible Factors (HIFs) (4). Among them -

[a]To whom correspondence should be addressed: ; Email: dervan@caltech.edu, California Institute of Technology, Division of Chemistry and Chemical Engineering, MC 164-30, Pasadena, California 91125.

[*]Current address: Jevgenij A. Raskatov, Dept. of Chemistry and Biochemistry, 1156 High St., University of California Santa Cruz, CA 95064

Conflicts of interest: The authors have no conflicts of interest to declare.

HIF-1 (5) - is a transcription factor that is often is associated with poorer patient survival (3). HIF-1 orchestrates numerous aspects of cancer progression - tumor angiogenesis, cell survival in hypoxia and metastasis (3, 6, 7). Most inhibitors affect HIF-1 signaling indirectly, by targeting other proteins, including Topoisomerase I, mammalian target of rapamycin (mTOR) or microtubules (7, 8). Established therapeutic strategies focus on modulating HIF-1 signaling by altering the HIF-1 protein levels (8), its dimerization and protein interactions (9–11), or its DNA binding and transcriptional activity (12–14).

One method to inhibit transcriptional activity of HIF-1 is to displace it from its DNA-binding site – HIF-1 responsive elements (HREs), for example by a molecule shown in this report (compound **1**. Fig. 1A) (12, 13). Compound **1** is a member of a class of DNA-binding small molecules – Pyrrole-Imidazole (Py-Im) polyamides - which can be programmed to recognize a broad repertoire of sequences with affinities and specificities comparable to those of transcription factors (15). We reported that polyamides can modulate gene expression driven by many transcription factors in tissue culture (12, 13, 16–18).

Experiments focused on HIF-1-DNA binding inhibition demonstrated the ability of **1** to displace the HIF-1 complex from DNA *in vitro* (12), and by reducing HIF-1a occupancy at selected HREs in a common tissue culture model of hypoxic response - U251 cells as represented in Fig. 1B (13). When U251 cells were treated with Deferoxamine, an iron chelator and HIF-1 activator (19), **1** was capable of inhibiting 23% of the induced genes, establishing polyamide **1** as a partial inhibitor of HIF-1 transcriptional activity (13). The concentration used was 1 μM, well below what was measured in the tumor tissues investigated in this study (2–3.5 μM). The overall gene expression changes included many important proangiogenic factors, such as *VEGFA*, *FLT1* or *Endothelin-1*, but also other factors. In light of the recent developments in cancer systems biology (20, 21) the broad effects of Py-Im polyamides on gene expression **1** (13, 16–18) led us to posit that their effects may arise due to affecting multiple targets. Recent discoveries show that drugs commonly act upon multiple molecular entities (20, 21) and this feature could be beneficial in cancer treatment thanks to decreased likelihood of developing drug resistance (22). However the potential for toxicity due to off target effects is a point of concern. Our mechanistic investigations expanded beyond the transcription factor:DNA interface and found that Py-Im polyamides can induce degradation of the large subunit of RNA polymerase II, activation of the P53 stress response without concurrent DNA damage (23) and induction of DNA replication stress (24).

We decided to establish whether the pattern of gene expression caused by administration of a Py-Im polyamide binding DNA sequence found in HREs (5′-WTWCG-3′) could result in measurable and useful anti-tumor effects *in vivo*. Our experiments focused on suppression of the phenotypes typical for tumor hypoxia, such as tumor vascularization, hypoxic gene expression or cancer cell survival (1, 8). We chose a subcutaneous tumor model, due to its hypoxic nature (3) and reliability of these measurements. The cell lines chosen for engraftment have been evaluated extensively in xenograft models of cancer (25, 26) and hypoxic gene expression in one of them (U251) can be regulated by **1** (13), making it a good choice for evaluating *in vivo* mechanism of action of **1**. The second cell line, GBM39 (27), was derived from the same site as U251 cells (brain), but was maintained as subcutaneous

xenografts and expanded in serum-free conditions as spheroids. The serum-free treatment maintains genetic and histologic variability of human tumors and was thus our choice to test generality of mechanism of action of polyamide **1** (28). Our previous *in vivo* investigations demonstrated the bioavailability of various Py-Im polyamides upon intravenous (29), intraperitoneal and subcutaneous administration (30). Subsequent *in vivo* xenograft studies established that polyamides could accumulate in subcutaneously grafted tumors (18, 30, 31), modulate tumor gene expression (18, 30) and inhibit growth of prostate cancer xenografts (23, 32). The distinct profile of gene expression modulation, favorable pharmacokinetics and ability to modulate all of the tested aspects of hypoxic response by **1**, could establish it as an interesting candidate for treatment of cancer and other hypoxia-related diseases. In the current study we established the ability of Py-Im polyamide 1 to interfere with hypoxic response, regulate gene expression in tumors and to inhibit tumor growth and angiogenesis.

Materials and methods

Cell Maintenance

U251 cell line was a kind gift of Dr. Giovanni Mellilo (NCI) in 2005. GBM39 cells were a gift of Dr. David Akhavan (UCLA) in 2013, originally obtained from Prof. David James (UCSF). The cell lines were authenticated using StemElite ID assay (Laragen). U251 cells were maintained in RPMI-1640 medium supplemented with 10% FBS. GBM39 cells were cultured in suspension in *F12/DMEM medium supplemented with b27, EGF (20 ng/ml) , FGF2 (20ng/ml), and Glutamax, heparin (50 μg/ml),* with growth factors replaced every two days. After 25 passages GBM39 were reestablished as subcutaneous xenografts (NSG mice). The tumor was disintegrated, digested in 10% accutase (3 h), cells resuspended by pipetting and then cultured as described above. Human umbilical vein endothelial cells (HUVECs) were cultured in 200 PRF medium (Gibco) supplemented with Low Serum Growth Supplement (LSGS, Invitrogen). Media was exchanged every 48 h and cells passaged weekly.

Tube formation assay

HUVECs were plated at 2×10^5 cells (75cm flask). After 36 hours, compound **1** (5 μM) was added for 72 h. Twelve-well plates were coated with 100 μl/well Geltrex (Invitrogen) and allowed to solidify at 37°C for 60 min. Cells were trypsinized and resuspended in 200 PRF medium at 2×10^5 mL^{-1}, and plated in the 12-well plates at 400 μL per well. After 6–12 hours the wells were imaged on an inverted microscope by selecting 4 random fields of view.

Pharmacokinetic and toxicity experiments

Animal experiments were carried out according to approved Institutional Animal Care and Use Committee protocols at the California Institute of Technology (Pasadena, CA). PK studies were done as previously described (30). Serum for analysis of toxicity markers (IDEXX) was obtained by RO collection and centrifugation (2000g, 15 min) in Serum Separator Tubes (BD Biosciences). The radioquantitation of **2** was performed as described elsewhere (33).

Immunohistochemistry and histologic analysis

Tissue processing was conducted at the Tissue Processing Core Laboratory (TPCL) at UCLA, using 5 μm paraffin sections. Tumor microvessels were visualized using anti-mouse CD31 staining using SC-1506 antibody (SCBT), apoptosis was assayed for using anti-human Cleaved-Caspase-3 (CC3) antibody (9664, CellSignal) and HIF-1a using CME 349A (Biocare Medical). At least two tissue sections per slide were used for each experiment. Slides were scanned using an Aperio ScanScope AT (Aperio) and positive pixel measurements were done using Imagescope software.

Perinecrotic area was defined as a field of view at 20× magnification that contained 50% necrosis and 50% adjacent, non-necrotic area, with edge of necrosis in the middle of the screen. Number of histologic measurements for each tissue section were chosen to limit variability of the final average value to <10%, per tumor, or until all available data in the section was counted. Ki-67 measurements were done using Immunoratio software at 20× magnification, with n=24 per tumor section. Nuclear density (and by proxy – necrosis) was assessed by automatic nuclei counting using Image-based Tool for Counting Nuclei (ITCN), 16 fields of view were analyzed per tumor section.

At least 6 (CC3), 9 (CD31), or 3 (TUNEL, GBM39), 5 (TUNEL, U251), or 8 (HIF) fields of view per tumor chosen randomly prior to analysis, at either 20× (CC3 staining, CD31 staining for U251, GBM39, Schedules A and B, TUNEL, HIF) or 40× magnification (CD31 staining for GBM39, *Schedule C*, due to higher CD31 positive vessel counts). For analysis of frequency of apoptotic blood vessels (CC3/CD31 double staining), we counted enough high power fields (20x) containing CD31 positive vessels, to assess at least 600 microvessels per condition.

Perinecrotic MVD was measured by first delineating nuclei on the edge of necrosis, and then offsetting the obtained path by an equivalent of 50 μm-350 μm in Illustrator CS5 (Adobe). The MVD was then counted manually for each 50 μm-zone and area integrated in Photoshop CS5 (Adobe). At least 40 measurements per tumor were obtained. Measurements of the nearest blood vessel-necrosis distance were done manually using Imagescope at 40× magnification.

Xenograft experiments

Experiments were carried out in 8–12 week old male NSG mice (NOD.Cg-Prkdcscid Il2rgtm1Wjl/SzJ, JAX). Cells were injected s.c. into a flank area (2.5×10^6 of U251 and 7.5×10^5 of GBM39 cells). U251 cells were administered in RPMI-1640 medium and GBM39 cells in 50% matrigel/culture medium. Before treatment, each vehicle-treated control xenograft was paired with a xenograft of the same initial volume to be treated with **1.** Compound was administered s.c. interscapularly in 20% DMSO/PBS. Mice were weighted weekly and euthanized if 15% weight loss, or more was observed.

Quantitative Real Time-Reverse Transcription-PCR assay

Primers (Supplementary Table 1) were designed using Harvard Primer bank (34). The total mRNA in tumors was processed as in our previous studies (30).

RNA-sequencing analysis

Cells for gene expression analysis were plated in 6-well plates at 5–10 × 10^4 cells per well and incubated in RPMI-1640 medium with 10% FBS until ~50% confluence (24–48 h). Afterward, medium was exchanged with the growth medium supplemented with **1** (1 μM). After 48 hours, either 300 μM of DFO, or PBS was supplemented, cells were incubated for an additional 16 hours. The RNA was then harvested using an RNEasy Kit (Qiagen) and treated with a Riboguard RNAse inhibitor and TurboDNA Free DNAse (Ambion), according to manufacturers' instructions. RNA-Seq libraries were prepared using standard Illumina reagents and protocols. Single read sequencing with the read length of 50 nucleotides was conducted on the Illumina HiSeq2000 sequencer, producing 35 to 40 million reads per library, with a total of three biological replicates per sample. Sequencing data were mapped against the combined human (hg19) transcriptome, using the Tophat2 program package 2.0.13 (35) and the GRCh37 annotation. Differential gene expression was calculated with the DEseq2 module (36). Clustering analysis was performed using Cluster 3.0 software (37).

Statistical analysis

Each sample was analyzed using a two-tailed, student’s t-test, assuming normality and unequal variance. P-value of 0.05 or less was considered statistically significant.

Results

Activity of Py-Im polyamide 1 depends on the HIF-1a activation

Our previous results showed that **1** can act as an inhibitor of HIF-1-driven gene expression (13) in U251 cells. However, we did not determine activity of **1** in cells without HIF-1a induction. Tumors contain both hypoxic and normoxic regions and thus it is important to establish how **1** acts in cells with and without induced HIF-1a. To address this question, U251 cells were first treated with **1** (1 μM, 48 h) or PBS (vehicle). Half of the samples were then dosed with a HIF-1a inducer Deferoxamine (DFO, 300 μM, 16 h), while the other half with PBS (Supplementary Figure 1A). Their mRNA was then analyzed by RNA-sequencing. Gene expression differences for each sample were obtained by normalizing a polyamide-treated sample with the appropriate non-treated control – cells treated with PBS and **1** were normalized to cells treated with PBS only (PBS vs **1**), and cells treated with both **1** and DFO to cells treated with DFO (DFO vs DFO+**1**). When **1** was dosed into cells treated with DFO, we observed it downregulated 744 genes. When **1** was dosed into cells dosed with PBS, a different set of genes was regulated. In fact only 101 out of 723 regulated genes were identical for both conditions (14%, Fig. 1C, D). The upregulated genes also varied between the two groups. Cells treated with **1** and DFO showed upregulation of 316 genes, while the same cells treated with **1** and PBS – 1514 genes. Few genes were in common between the two groups (6% for DFO, 1.3% for PBS, Fig. 1C, D). Overall, 17% DFO-induced genes were downregulated by **1** at least 2-fold ($p < 0.05$). Gene clustering analysis suggested **1** acted to reverse effects of DFO (Supplementary Figure 1B–C). Fewer genes were affected by compound **3** at the same dose (Supplementary Figure 1D). Interestingly, we found that among the genes that were changed significantly both by **1** (in DFO-induced cells) and by DFO, the Py-Im polyamide **1** inhibited DFO-induced gene expression in 96% of the genes

(2557 out of 2661 genes, Supplementary Figure 1E). This indicates that gene expression changes caused by DFO, are either unaffected, or reversed by **1**, but rarely, if ever, exacerbated by treatment with **1**.

Py-Im polyamide 1 shows favorable preliminary pharmacokinetics and tissue distribution at tolerable doses

In order to evaluate bioavailability of **1** *in vivo*, we injected it subcutaneously (s.c.) at 6.8 mg/kg into C57BL6 mice. Compound **1** reached a serum concentration of 11.3±1.6 μM within 1.5 h and 7.8±0.4 μM at 4 h post-injection (n=4, Fig. 2A). The radiolabeled analogue of **1**, Py-Im polyamide **2**, was injected intraperitoneally (IP) to quantitate whole-organ compound concentrations (n=6, Supplementary Figure 2A, B) into immunocompromised NSG mice bearing GBM39 tumors. After 24 h, concentrations of **2** were measured in GBM39 xenografts (2.0 μM), host's kidney (6.3 μM), liver (4.2 μM) and lung (3.1 μM; Supplementary Figure 2A). Following 3 injections (6.8 mg/kg s.c., every other day × 3, harvest 24h post last injection), all tested tissues showed compound accumulation (Supplementary Figure 2B). The same administration of **3** (FITC-conjugate of **1**) in NSG mice resulted in readily detectable nuclear staining in tumor cells and tested tissue sections (Supplementary Figure 2C–E). The nuclear staining was also present when tested in unfixed cells in tissue culture setting (Fig. 2B). A single-injection toxicity test showed that **1** did not affect animal weight, or levels of serum toxicity markers (ALT, AST, TBIL, BUN, Creatinine) at concentrations up to 10 mg/kg (Supplementary Figure 3A, B). Taken together, these results supported evaluation of anti-tumor effects of **1** *in vivo*.

Polyamide 1 suppresses tumor growth in subcutaneous xenografts

To test whether previously established partial inhibition of HIF-1-driven gene expression by **1** (13) would result in decrease in tumor growth, we engrafted U251 and GBM39 cells s.c. into NOD/SCID-γ (NSG) mice. We established three dosing regiments (Supplementary Figure 4A) for **1** – *Schedule A*, consisting of three s.c. injections every other day at maximum tolerated dose (6.8 mg/kg, 8 days) and *Schedules B and C*, with lower dose (4.5mg/kg, 3 inj./week) designed for prolonged treatment with low weight loss (<10%) over 4 weeks (U251 tumors) or 6 weeks (GBM39 tumors). The S*chedule A* was designed to elicit maximum response over a short period of time at a dose tolerable to animals. The *Schedules B* and *C* were introduced to assess if the compound **1** could retain its activity at a dose that could be tolerated over longer periods of time. In all cases, the tumors were harvested 72 h after last injection, due to our previous research, indicating that Py-Im polyamide-induced apoptosis occurs between 48–72 hours after compound administration in tissue culture studies (24).

Mice bearing U251 tumors were subjected to treatment with **1** (*Schedule A*) which resulted in a reduction in median tumor mass (1.8-fold, $p<0.013$; n=7, 8 for vehicle and treated groups; Fig. 2C) compared to vehicle. Similarly, prolonged treatment (*Schedule B*) resulted in 1.9-fold lower median U251 tumor mass ($p<0.0125$; n=10 per condition; Fig. 2D). Consistent results were obtained with a primary glioma cell line (GBM39) xenograft. Treatment according to *Schedule A* resulted in 1.8-fold lower median mass ($p<0.016$; n=11 per condition; Supplementary Figure 4B) and prolonged treatment (*Schedule C*) in 1.6-fold

reduction ($p<0.041$; n=6 per condition; Supplementary Figure 4C). The treatments resulted in minor mouse weight loss; the effects were less severe (<5% average w.l. throughout the experiment) for schedules *B* and *C* (Supplementary Figure 5).

Polyamide 1 reduces microvessels density in xenografts, without inducing endothelial apoptosis

Hypoxic signaling is a major driver for angiogenesis and its inhibition leads to decrease in microvessel density (MVD) (1, 8). We measured MVD using anti-mouse CD31 immunostaining of tumor sections. We observed a significant reduction of MVD in all tested scenarios. For U251 tumors, with mice subjected to *Schedule A,* we observed a 1.4-fold median reduction of MVD ($p<0.014$; n=7, 8 for vehicle and treated groups; Fig. 2E) and 1.7-fold median decrease for *Schedule B* ($p<0.05$; n=10 per condition; Fig. 2F). For GBM39 tumors, both treatment schedules (*A* and *C*) led to 1.4-fold reduction in MVD ($p <0.01$; n=11 and n=6 for Schedules *A* and *C*; Supplementary Figure 6A–B).

The decrease in MVD could be caused by direct effect of **1** on the endothelium, for example, rendering it either apoptotic, or unable to form blood vessels. We evaluated endothelial apoptosis by double-staining of mouse-specific CD31 and Cleaved Caspase-3 (CC3) in GBM39 tumors (*Schedule C*; n=5 tumors, approximately 600 microvessels per condition; Fig. 2G). We found no significant endothelial apoptosis in either of the treatment groups. To measure angiogenic functionality of endothelium we used *in vitro* matrigel tube formation assay with Human Umbilical Cord Endothelial Cells (HUVEC), revealing **1** (5 μM, 48 h) had no effect on tube formation (n=3, Fig. 2H).

Antiangiogenic effects of 1 are associated with inhibition of hypoxic response

Decrease in MVD, without endothelial apoptosis or dysfunction, suggests **1** could interfere with the hypoxic response (5). To further test this hypothesis we evaluated other aspects affected by hypoxic response, such as tumor cell proliferation (38), apoptosis in HIF-1 positive, perinecrotic areas (38), nuclear HIF-1a protein accumulation and cell survival in areas distant from blood vessels (39, 40). To analyze this, we divided the tumor sections into three areas: necrotic, non-necrotic and perinecrotic (Fig. 3A). The non-necrotic areas contain nucleated cells with intact cell membranes, while necrotic areas are show loss of nuclei and fragmentation of cells. The perinecrotic area represents field of view (20× magnification) that contains 50% of cells containing nuclei and 50% of necrotic areas.

Antiangiogenic therapy increases hypoxia in tumors and often leads to decreased proliferation (39, 41). Upon treatment with **1** (*Schedule B*), we observed a 1.2-fold decrease ($P<0.05$; n=10 per condition; Fig. 3B) in proliferation marker (Ki-67) in non-necrotic areas of the U251 tumors.

Another effect of induction of hypoxic response is accumulation of HIF-1a (1). However, treatment with **1** did not lead to increase in levels of HIF-1a in either U251 (Fig. 3C, D) or GBM39 (Supplementary Figure 7A, B) tumors. Lack of HIF-1a accumulation is unlikely to be caused by its increased degradation, as **1** does not affect HIF-1a levels in tissue culture (Supplementary Figure 7C). Overall, we observed a spatial distribution of HIF-1a in U251

tumor sections – perinecrotic areas showed higher HIF-1a levels compared to non-necrotic areas (1.8-fold average increase for **1**, $p<0.001$; n=10 per condition; Fig. 3C, D).

Induction of hypoxic signaling can lead to apoptosis resistance in cancer cells (39). However, treatment with **1** increased apoptosis significantly in perinecrotic, HIF-1a positive, areas (CC3 staining, 1.8-fold, $p<0.0012$; n=10 per condition; Fig. 3E;). The apoptosis was absent in non-necrotic regions of U251 tumors regardless of the treatment (Fig. 3F), suggesting **1** is toxic specifically to hypoxic cells. Similarly, TUNEL staining revealed convergent results – no increase in apoptotic cells in non-necrotic regions, and 1.7-fold ($p<0.009$, n=10 per condition) increase in apoptosis in perinecrotic tumor regions upon treatment with **1** (Supplementary Figure 7D–E). The GBM39 tumors harvested before they developed necrosis also revealed no induction of apoptosis by **1** (Supplementary Figure 7F).

Hypoxic signaling mediates cell survival in areas with low oxygen pressures. With increasing distance to blood vessels, tumor necrosis appears as a result of the death of cells with inadequate oxygen supply (1, 42). The oxygen pressure decreases as the function of distance from blood vessels, and typically does not reach beyond approximately 200 μm. Cells adapt to low oxygen pressures by activating hypoxic signaling, and once oxygen pressures drop below a critical value, cell necrosis occurs (1, 42). The cells that succeed to survive at distances comparable to 200 μm from blood vessels, can thus be deemed as having a functional hypoxic response. Impairment of hypoxic signaling will result in necrosis occurring at higher oxygen pressures – at shorter distances from blood vessels. Therefore to measure if **1** decreases ability of cells to adapt to low oxygen pressures, we measured MVD as a function of distance from the edge of necrotic areas. We found the expected lack of microvessels near necrotic edges (<100 μm). In tumors derived from animals treated with **1** (U251, *Schedule B*) necrotic edge appeared closer to the blood vessels. The median distances between the edge of necrosis and the nearest blood vessels, were significantly shorter for both U251 and GBM39 tumors treated with **1**, as compared to vehicle-treated controls ($p<0.01$, Supplementary Figure 7G). Similarly, at short distances around necrosis the mean MVD appeared higher for tumors treated with **1,** suggesting treated tumor cells require higher level of nutrients and oxygen for survival (3.3-fold at 150 μm and 2.3-fold for 200 μm distance from the necrotic edge, $p<0.02$ and $p<0.01$; Fig. 4A, B).

Lower MVD and lower cell survival at a distance from blood vessels, should lead to an increase in necrotic area. However, the complex pattern of necrosis (micronecroses) in U251 tumors made it difficult to quantify it by a simple delineation. Instead, we decided to automatically count nuclei in the whole tumor section and found lower nuclear density in tumors treated with **1**, (10% fewer nuclei, $p<0.03$, Supplementary Figure 8A). The further evidence of necrosis induction by **1**, was present after short-term treatment with **1** in GBM39 tumors (*Schedule A*) where transient accumulation of HIF-1a (Supplementary Figure 8B–D) led to presence of necrosis (Supplementary Figure 8E), specifically localized to HIF-1a positive areas that were distant from microvessels (Supplementary Figure 8E, F).

Overall, compound **1** decreases proliferation and nuclear density, selectively induces apoptosis in perinecrotic, HIF-1a positive areas, and causes necrotic areas to appear in

proximity of blood vessels despite the presence of a blood supply, but treatment does not result in long-term HIF-1a accumulation.

Py-Im polyamide 1 reduces expression of proangiogenic and prometastatic factors *in vivo*

A common adverse effect of antiangiogenic treatment is upregulation of proangiogenic and prometastatic gene expression which renders the antiangiogenic therapies less effective and is often a result of hypoxic signaling (43). We decided to test if **1** affected mRNA expression of such factors *in vivo*. NSG mice bearing U251 tumors were treated with **1** according to *Schedule D* (6.8 mg/kg, 2 inj., on days 1 and 3; tumors harvested on day 5; SI Supplementary Figure 4A). Out of 10 tested proangiogenic factors, four transcripts had lower relative expression after treatment with **1** (Fig. 5A), and one (*VEGFA*) was upregulated (1.4-fold) in both mRNA (Fig. 5B) and serum protein levels (Fig. 5C). Downregulation of mRNA expression was also apparent in the panel of prometastatic genes. Overall, 5 out of 6 tested transcripts were downregulated in the group treated with **1** (Fig. 5D). The factors significantly affected by **1**, included: *FLT1, NLGN1, HOXB9, NEDD9, MMP2* and *MMP14*. Interestingly, the mouse receptor of Angiopoietin, *Tek,* was also downregulated. Results for all tested genes can be found in Supplementary Table 2.

Discussion

Regulation of hypoxic signaling is central to maintaining balance between health and disease. Its principal regulator - HIF-1 - is essential for tumor initiation and progression, *e.g.* vascularization, cell survival and metastasis (3, 44). Inhibition of HIF-1 activity has suppressed tumor progression and reduced cancer resistance to available therapies (reviewed in (1, 3)). Our group has previously reported on the function of an HRE-binding Py-Im polyamide **1** as a partial inhibitor of HIF-1 dependent transcription in tissue culture (13). However, the *in vivo* activity and mechanism of **1** remained to be explored. We used Py-Im polyamide **1** (Fig. 1) to show its activity is dependent on HIF-1a activation (Fig. 1), that it inhibits tumor growth, angiogenesis (Fig. 2) and the tested aspects of hypoxic response *in vivo* (Figs. 3 and 4), including inhibition of tumor-derived mRNA expression of proangiogenic and prometastatic factors that are often upregulated in hypoxic conditions (Fig. 5). We found that the effects of **1** are consistent with what would be expected in case of a partial inhibition of hypoxic response (Fig. 6).

Polyamide tissue distribution and preliminary pharmacokinetics

Subcutaneous administration revealed **1** distributes into serum within 1.5 h post-injection, with 31% drop in concentration 2.5 h later, indicating multi-hour long half-life. Even though **1** had favorable pharmacokinetics, its activity *in vivo* is likely dependent on the target tissue concentration. After three intraperitoneal injections (Schedule *A*), the radioactive analog **2** reached a concentration of 3.5 μM in GBM39 tumor and higher levels in other tissues. Concentrations attained for **1** in all tested tissues were thus higher than used in our tissue culture studies (13).

Effects on tumor growth and vascularization

In the present study, inhibition of tumor growth and reduction in MVD was observed in two different cell types in response to treatment with **1**. The extent of these effects was comparable to ones exerted by Bevacizumab (45) in xenografts derived from U251 (41) and GBM39 cells (26). Investigation of possible mechanisms of antiangiogenic action showed lack of apoptosis in blood vessel lining, and no measurable influence on tube formation on matrigel. Lack of direct effects of **1** on endothelial cells suggests blood vessel recruitment might be impaired. One possible explanation is inhibition of expression of tumor-associated proangiogenic factors by **1**. However, systemic concentration of those proteins could also be affected.

Effects on apoptosis, proliferation and HIF-1a levels

Compound **1** induces apoptosis selectively, in HIF-1a-positive, perinecrotic areas. This suggests **1** sensitizes cancer cells to hypoxia, which could occur by hypoxic response inhibition (3). Our RNA-sequencing data shows that activity of 1 depends on activation of HIF-1a, which provides a possible explanation why activity of **1** was restricted to cells in HIF-1a positive areas. Further support of this hypothesis is the lack of increase of HIF-1a positive cells in the tumors treated according to *Schedule B* and *C*. Since **1** did not affect HIF-1a levels in U251 cells in tissue culture, it is likely that numbers of HIF-1a positive cells were reduced as they went through apoptosis. Finally, increased reliance of cancer cells on proximity to vasculature once again suggests their hindered ability to adapt to low partial oxygen pressures, which is the main function of the hypoxic response. It is worth noting that, despite the fact that more blood vessels exist in proximity of necrosis, the perinecrotic areas are not representative of the whole tumor. These areas contain only a small fraction of tumor area and inherently contain few blood vessels, which leads to necrosis. The transient induction of HIF-1a levels in briefly-treated GBM39 tumors indicates a likely increase in tumor hypoxia, or a change in HIF-1a protein levels by direct action of **1**. The latter possibility is unlikely as **1** had no effect on HIF-1a levels in tissue culture. The apparent disparity in HIF-1a levels between the GBM39 tumors treated according to *Schedule A*, and other regimens, could be due to two factors: concentration of **1** was insufficient to induce apoptosis of tumor cells in *Schedule A*, or overall level of hypoxia in these smaller tumors (Supplementary Figure 8C) was too low to induce sensitivity to **1**. The latter hypothesis is supported by comparable HIF-1a levels in non-necrotic regions of GBM39 tumors from a group treated according to *Schedule C* (Supplementary Figure 7A) and by tendency of smaller tumors to be less hypoxic (46). Reduced proliferation upon treatment with **1** is likely a combination of both reduced MVD and a direct effect of 1 on cancer cells. The former hypothesis is supported by the dependence of proliferation on distance from necrosis, while the latter – by a reduction in Ki-67 in non-necrotic areas that are presumably sufficiently vascularized for unrestricted cell division.

Effects on gene expression

Compound **1** reduced mRNA expression of a panel of genes involved in angiogenesis and metastasis. Many of the affected genes carry important functions in tumor adaptation to hypoxia – for example Platelet-derived growth factor subunit B (*PDGFB*) and

Angiopoietin-1 (*ANGPT1*) are involved in blood vessel maturation (43), whereas Lysyl Oxidase (*LOX*) or *RHOC* were involved in metastasis (47, 48). Other factors significantly affected by **1**, included: *FLT1, NLGN1, HOXB9, NEDD9, MMP2* and *MMP14*, and a mouse Angiopoietin receptor, *Tek*. We also observed a slight elevation (1.4-fold) in both mRNA expression and serum concentration of VEGFA, despite a visible downregulation in tissue culture (13). Reduction in microvessel density typically leads to decreased oxygen pressure and increased expression of proangiogenic factors, including VEGFA (41, 43). Interestingly, recent studies show that regulation of VEGFA activity can be HIF-1-independent (49, 50). However, it is also possible that VEGFA expression would be higher had it not been for treatment with **1**. Importantly, elevated expression of VEGFA did not prevent **1** from exerting antiangiogenic effect, suggesting its mechanism of action could be VEGF-independent.

Conclusions

In summary, this study demonstrates that Py-Im polyamide **1** interferes with the tested endpoints of hypoxic response in tumors: it inhibits prometastatic and proangiogenic gene expression, induces tumor cell apoptosis selectively in HIF-1a positive areas and decreases nuclear density, proliferative index and microvessel density of tumors. The RNA-sequencing data revealed that **1** regulates genes differentially in cells with induced and basal levels of HIF-1a, providing a potential explanation for selective induction of apoptosis in HIF-1a positive cells. This compound could be useful in treatment of hypoxia-related disease as it distributes to tissues, has favorable pharmacokinetics, and antitumor and antiangiogenic activity in two different xenografts.

Supplementary Material

Refer to Web version on PubMed Central for supplementary material.

Acknowledgments

The authors thank Caltech OLAR for technical assistance with animal experiments and TPCL (UCLA) for assisting with IHC. The authors thank Dr. Nora Rozengurt (UCLA) for helpful suggestions, discussion and preliminary pathological evaluation of tumor sections. We thank Drs. Nicholas Nickols and Bogdan Olenyuk for helpful discussions and suggestions.

Financial support: This work was supported by the NIH Grant GM-51747. J.O.Szablowski. was supported by NIH GM-51747. J.A.Raskatov received postdoctoral support from the Alexander von Humboldt foundation.

References

1. Semenza GL. Oxygen sensing, hypoxia-inducible factors, and disease pathophysiology. Annu Rev Pathol. 2014; 9:47–71. [PubMed: 23937437]
2. Siegel R, Naishadham D, Jemal A. Cancer statistics, 2013. CA Cancer J Clin. 2013 Jan; 63(1):11–30. [PubMed: 23335087]
3. Wilson WR, Hay MP. Targeting hypoxia in cancer therapy. Nat Rev Cancer. 2011 Jun; 11(6):393–410. [PubMed: 21606941]
4. Semenza GL, Nejfelt MK, Chi SM, Antonarakis SE. Hypoxia-inducible nuclear factors bind to an enhancer element located 3′ to the human erythropoietin gene. Proc Natl Acad Sci U S A. 1991 Jul 1; 88(13):5680–4. [PubMed: 2062846]

5. Wang GL, Jiang BH, Rue EA, Semenza GL. Hypoxia-inducible factor 1 is a basic-helix-loop-helix-PAS heterodimer regulated by cellular O2 tension. Proc Natl Acad Sci U S A. 1995 Jun 6; 92(12): 5510–4. [PubMed: 7539918]
6. Brown JM, Wilson WR. Exploiting tumour hypoxia in cancer treatment. Nat Rev Cancer. 2004 Jun; 4(6):437–47. [PubMed: 15170446]
7. Li L, Kaelin WG Jr. New insights into the biology of renal cell carcinoma. Hematol Oncol Clin North Am. 2011 Aug; 25(4):667–86. [PubMed: 21763962]
8. Onnis B, Rapisarda A, Melillo G. Development of HIF-1 inhibitors for cancer therapy. J Cell Mol Med. 2009 Sep; 13(9A):2780–6. [PubMed: 19674190]
9. Kung AL, Zabludoff SD, France DS, Freedman SJ, Tanner EA, Vieira A, et al. Small molecule blockade of transcriptional coactivation of the hypoxia-inducible factor pathway. Cancer Cell. 2004 Jul; 6(1):33–43. [PubMed: 15261140]
10. Lao BB, Grishagin I, Mesallati H, Brewer TF, Olenyuk BZ, Arora PS. In vivo modulation of hypoxia-inducible signaling by topographical helix mimetics. Proc Natl Acad Sci U S A. 2014 May 27; 111(21):7531–6. [PubMed: 24821806]
11. Lee K, Zhang H, Qian DZ, Rey S, Liu JO, Semenza GL. Acriflavine inhibits HIF-1 dimerization, tumor growth, and vascularization. Proc Natl Acad Sci U S A. 2009 Oct 20; 106(42):17910–5. [PubMed: 19805192]
12. Olenyuk BZ, Zhang GJ, Klco JM, Nickols NG, Kaelin WG Jr, Dervan PB. Inhibition of vascular endothelial growth factor with a sequence-specific hypoxia response element antagonist. Proc Natl Acad Sci U S A. 2004 Nov 30; 101(48):16768–73. [PubMed: 15556999]
13. Nickols NG, Jacobs CS, Farkas ME, Dervan PB. Modulating hypoxia-inducible transcription by disrupting the HIF-1-DNA interface. ACS Chem Biol. 2007 Aug 17; 2(8):561–71. [PubMed: 17708671]
14. Lee K, Qian DZ, Rey S, Wei H, Liu JO, Semenza GL. Anthracycline chemotherapy inhibits HIF-1 transcriptional activity and tumor-induced mobilization of circulating angiogenic cells. Proc Natl Acad Sci U S A. 2009 Feb 17; 106(7):2353–8. [PubMed: 19168635]
15. Hsu CF, Phillips JW, Trauger JW, Farkas ME, Belitsky JM, Heckel A, et al. Completion of a Programmable DNA-Binding Small Molecule Library. Tetrahedron. 2007 Jul 2; 63(27):6146–51. [PubMed: 18596841]
16. Nickols NG, Dervan PB. Suppression of androgen receptor-mediated gene expression by a sequence-specific DNA-binding polyamide. Proc Natl Acad Sci U S A. 2007 Jun 19; 104(25): 10418–23. [PubMed: 17566103]
17. Raskatov JA, Meier JL, Puckett JW, Yang F, Ramakrishnan P, Dervan PB. Modulation of NF-kappaB-dependent gene transcription using programmable DNA minor groove binders. Proc Natl Acad Sci U S A. 2012 Jan 24; 109(4):1023–8. [PubMed: 22203967]
18. Nickols NG, Szablowski JO, Hargrove AE, Li BC, Raskatov JA, Dervan PB. Activity of a Py-Im polyamide targeted to the estrogen response element. Mol Cancer Ther. 2013 May; 12(5):675–84. [PubMed: 23443804]
19. Kaelin WG Jr, Ratcliffe PJ. Oxygen sensing by metazoans: the central role of the HIF hydroxylase pathway. Mol Cell. 2008 May 23; 30(4):393–402. [PubMed: 18498744]
20. Du W, Elemento O. Cancer systems biology: embracing complexity to develop better anticancer therapeutic strategies. Oncogene. 2014 Sep 15.
21. Yildirim MA, Goh KI, Cusick ME, Barabasi AL, Vidal M. Drug-target network. Nat Biotechnol. 2007 Oct; 25(10):1119–26. [PubMed: 17921997]
22. Mencher SK, Wang LG. Promiscuous drugs compared to selective drugs (promiscuity can be a virtue). BMC Clin Pharmacol. 2005; 5:3. [PubMed: 15854222]
23. Yang F, Nickols NG, Li BC, Marinov GK, Said JW, Dervan PB. Antitumor activity of a pyrrole-imidazole polyamide. Proc Natl Acad Sci U S A. 2013 Jan 29; 110(5):1863–8. [PubMed: 23319609]
24. Martinez TF, Phillips JW, Karanja KK, Polaczek P, Wang CM, Li BC, et al. Replication stress by Py-Im polyamides induces a non-canonical ATR-dependent checkpoint response. Nucleic Acids Res. 2015; 42(18):11546–59. [PubMed: 25249630]

25. Jacobs VL, Valdes PA, Hickey WF, De Leo JA. Current review of in vivo GBM rodent models: emphasis on the CNS-1 tumour model. ASN Neuro. 2011; 3(3):e00063. [PubMed: 21740400]
26. Hu YL, DeLay M, Jahangiri A, Molinaro AM, Rose SD, Carbonell WS, et al. Hypoxia-induced autophagy promotes tumor cell survival and adaptation to antiangiogenic treatment in glioblastoma. Cancer Res. 2012 Apr 1; 72(7):1773–83. [PubMed: 22447568]
27. Sarkaria JN, Carlson BL, Schroeder MA, Grogan P, Brown PD, Giannini C, et al. Use of an orthotopic xenograft model for assessing the effect of epidermal growth factor receptor amplification on glioblastoma radiation response. Clin Cancer Res. 2006 Apr 1; 12(7 Pt 1):2264–71. [PubMed: 16609043]
28. Tentler JJ, Tan AC, Weekes CD, Jimeno A, Leong S, Pitts TM, et al. Patient-derived tumour xenografts as models for oncology drug development. Nat Rev Clin Oncol. 2012 Jun; 9(6):338–50. [PubMed: 22508028]
29. Synold TW, Xi B, Wu J, Yen Y, Li BC, Yang F, et al. Single-dose pharmacokinetic and toxicity analysis of pyrrole-imidazole polyamides in mice. Cancer Chemother Pharmacol. 2012 Oct; 70(4): 617–25. [PubMed: 22907527]
30. Raskatov JA, Hargrove AE, So AY, Dervan PB. Pharmacokinetics of Py-Im polyamides depend on architecture: cyclic versus linear. J Am Chem Soc. 2012 May 9; 134(18):7995–9. [PubMed: 22509786]
31. Raskatov JA, Szablowski JO, Dervan PB. Tumor xenograft uptake of a pyrrole-imidazole (Py-Im) polyamide varies as a function of cell line grafted. J Med Chem. 2014 Oct 23; 57(20):8471–6. [PubMed: 25238175]
32. Yang F, Nickols NG, Li BC, Szablowski JO, Hamilton SR, Meier JL, et al. Animal toxicity of hairpin pyrrole-imidazole polyamides varies with the turn unit. J Med Chem. 2013 Sep 26; 56(18): 7449–57. [PubMed: 24015881]
33. Raskatov JA, Puckett JW, Dervan PB. A C-14 labeled Py-Im polyamide localizes to a subcutaneous prostate cancer tumor. Bioorg Med Chem. 2014 Aug 15; 22(16):4371–5. [PubMed: 24780272]
34. Spandidos A, Wang X, Wang H, Seed B. PrimerBank: a resource of human and mouse PCR primer pairs for gene expression detection and quantification. Nucleic Acids Res. 2010 Jan; 38(Database issue):D792–9. [PubMed: 19906719]
35. Kim D, Pertea G, Trapnell C, Pimentel H, Kelley R, Salzberg SL. TopHat2: accurate alignment of transcriptomes in the presence of insertions, deletions and gene fusions. Genome Biology. 2013; 14(4)
36. Love MI, Huber W, Anders S. Moderated estimation of fold change and dispersion for RNA-seq data with DESeq2. Genome Biology. 2014; 15(12)
37. de Hoon MJ, Imoto S, Nolan J, Miyano S. Open source clustering software. Bioinformatics. 2004 Jun 12; 20(9):1453–4. [PubMed: 14871861]
38. Vaupel P, Mayer A. Hypoxia in cancer: significance and impact on clinical outcome. Cancer Metastasis Rev. 2007 Jun; 26(2):225–39. [PubMed: 17440684]
39. Blagosklonny MV. Antiangiogenic therapy and tumor progression. Cancer Cell. 2004 Jan; 5(1):13–7. [PubMed: 14749122]
40. Tang CM, Yu J. Hypoxia-inducible factor-1 as a therapeutic target in cancer. J Gastroenterol Hepatol. 2013 Mar; 28(3):401–5. [PubMed: 23173651]
41. Rapisarda A, Hollingshead M, Uranchimeg B, Bonomi CA, Borgel SD, Carter JP, et al. Increased antitumor activity of bevacizumab in combination with hypoxia inducible factor-1 inhibition. Mol Cancer Ther. 2009 Jul; 8(7):1867–77. [PubMed: 19584228]
42. Thomlinson RH, Gray LH. The histological structure of some human lung cancers and the possible implications for radiotherapy. Br J Cancer. 1955 Dec; 9(4):539–49. [PubMed: 13304213]
43. Loges S, Schmidt T, Carmeliet P. Mechanisms of resistance to anti-angiogenic therapy and development of third-generation anti-angiogenic drug candidates. Genes Cancer. 2010 Jan; 1(1): 12–25. [PubMed: 21779425]
44. Ryan HE, Lo J, Johnson RS. HIF-1 alpha is required for solid tumor formation and embryonic vascularization. EMBO J. 1998 Jun 1; 17(11):3005–15. [PubMed: 9606183]

45. Presta LG, Chen H, O'Connor SJ, Chisholm V, Meng YG, Krummen L, et al. Humanization of an anti-vascular endothelial growth factor monoclonal antibody for the therapy of solid tumors and other disorders. Cancer Res. 1997 Oct 15; 57(20):4593–9. [PubMed: 9377574]

46. Lyng H, Skretting A, Rofstad EK. Blood flow in six human melanoma xenograft lines with different growth characteristics. Cancer Res. 1992 Feb 1; 52(3):584–92. [PubMed: 1732046]

47. Erler JT, Bennewith KL, Nicolau M, Dornhofer N, Kong C, Le QT, et al. Lysyl oxidase is essential for hypoxia-induced metastasis. Nature. 2006 Apr 27; 440(7088):1222–6. [PubMed: 16642001]

48. Sethi N, Kang Y. Unravelling the complexity of metastasis - molecular understanding and targeted therapies. Nat Rev Cancer. 2011 Oct; 11(10):735–48. [PubMed: 21941285]

49. Arany Z, Foo SY, Ma Y, Ruas JL, Bommi-Reddy A, Girnun G, et al. HIF-independent regulation of VEGF and angiogenesis by the transcriptional coactivator PGC-1alpha. Nature. 2008 Feb 21; 451(7181):1008–12. [PubMed: 18288196]

50. Mizukami Y, Kohgo Y, Chung DC. Hypoxia inducible factor-1 independent pathways in tumor angiogenesis. Clin Cancer Res. 2007 Oct 1; 13(19):5670–4. [PubMed: 17908955]

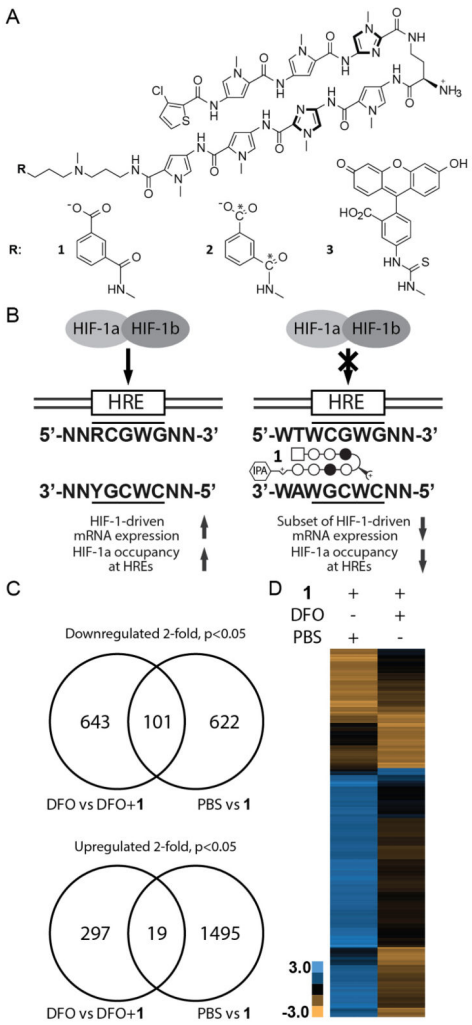

Figure 1. Chemical structure and biological activity of Py-Im polyamides binding HRE sequence

A) Chemical structures and ball-and-stick representation of the Py-Im polyamides **1**–**3**. N-methyl-pyrrole, N-methyl-imidazole and chlorothiophene are represented as open circles, filled circles and squares, respectively. B) Our previous studies (13) indicated that compound **1** can bind to HRE-containing sequence with sub-nanomolar ($k_a > 10^{10}$) affinity and displace HIF-1 complex from VEGFA and CA9 promoters in U251 cells in Chromatin Immuno-Precipitation assay (ChIP). C) Gene expression regulation by **1** (1 μM) in U251 cells with elevated levels of HIF-1a (treatment with 300 μM Deferoxamine (DFO)) or native levels of HIF-1a (PBS treatment). Cells were treated either with PBS or **1** for 48 hours, and then with either PBS or DFO for 16 hours. Gene expression changes for each sample were obtained by normalizing a polyamide-treated sample with the appropriate non-treated control – cells treated with PBS and **1** were normalized to cells treated with PBS only, and cells treated with both **1** and DFO were normalized to cells treated with DFO. Overall, **1** regulates expression of a distinct set of genes when cells are co-treated with DFO and **1**. D) Hierarchical clustering (Euclidian distance, complete linkage) of genes changed at least

three-fold as compared to the state untreated with **1**. Gene expression changes expressed as Log_2 values. Three biological replicates were analyzed.

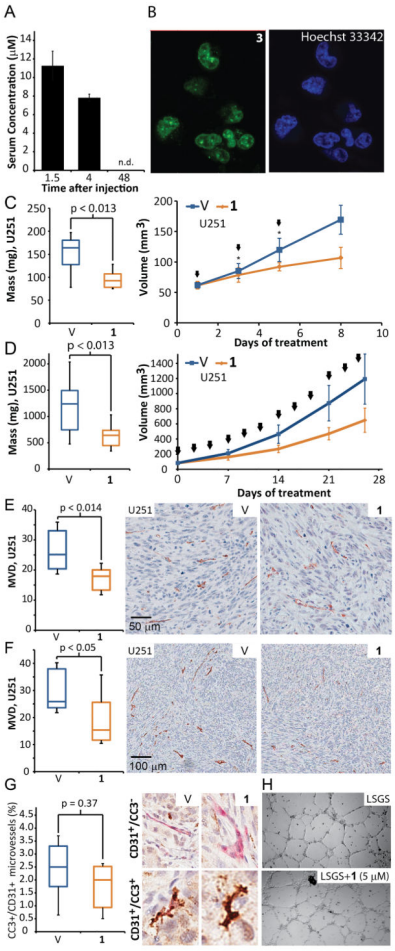

Figure 2. Polyamide 1 inhibits tumor growth and vascularization after systemic administration

A) Serum concentration of **1** after subcutaneous injection. The C57BL6 mice were injected with **1** subcutaneously into interscapular area, after which we drew blood via retroorbital collection (n=4 per time point). B) Nuclear uptake of **3** in U251 cells, counterstained with a DNA-binding Hoechst 33342 fluorophore. C) Final masses and growth curve of s.c. U251 xenografts derived from animals subjected to *Schedule A* (n=7,8, for vehicle and treated groups; for volumes, measurements at the 3rd an 5th day contain 5 data points.) D) Final masses and growth curve of U251 xenografts (*Schedule B*, n=10 per condition). E) Mice harboring xenografts were treated with **1** according to *Schedule A* and their MVD score was measured using anti-mouse CD31 immunostaining of tumor sections (For U251 n=7,8 for vehicle, and treated groups). F) Prolonged treatments, according to *Schedule B* in U251 xenografts led to comparable decrease in MVD. G) Apoptosis in blood vessels was determined by double-staining of Cleaved Caspase-3 (CC3) and mouse CD31 of GBM39 tumor sections treated according to *Schedule C*. Both vehicle and polyamide-**1** treated samples exhibited low levels of blood vessel apoptosis and the differences between the groups were not significant (p=0.37, n=5 per condition). H) An in vitro angiogenesis assay - matrigel tube formation assay using HUVECs - shows treatment with **1** (5 μM) over 48h has no effect on endothelial tube formation. Arrows denote injections. Error bars are 95% CI for growth curves and minimum-maximum for other graphs.

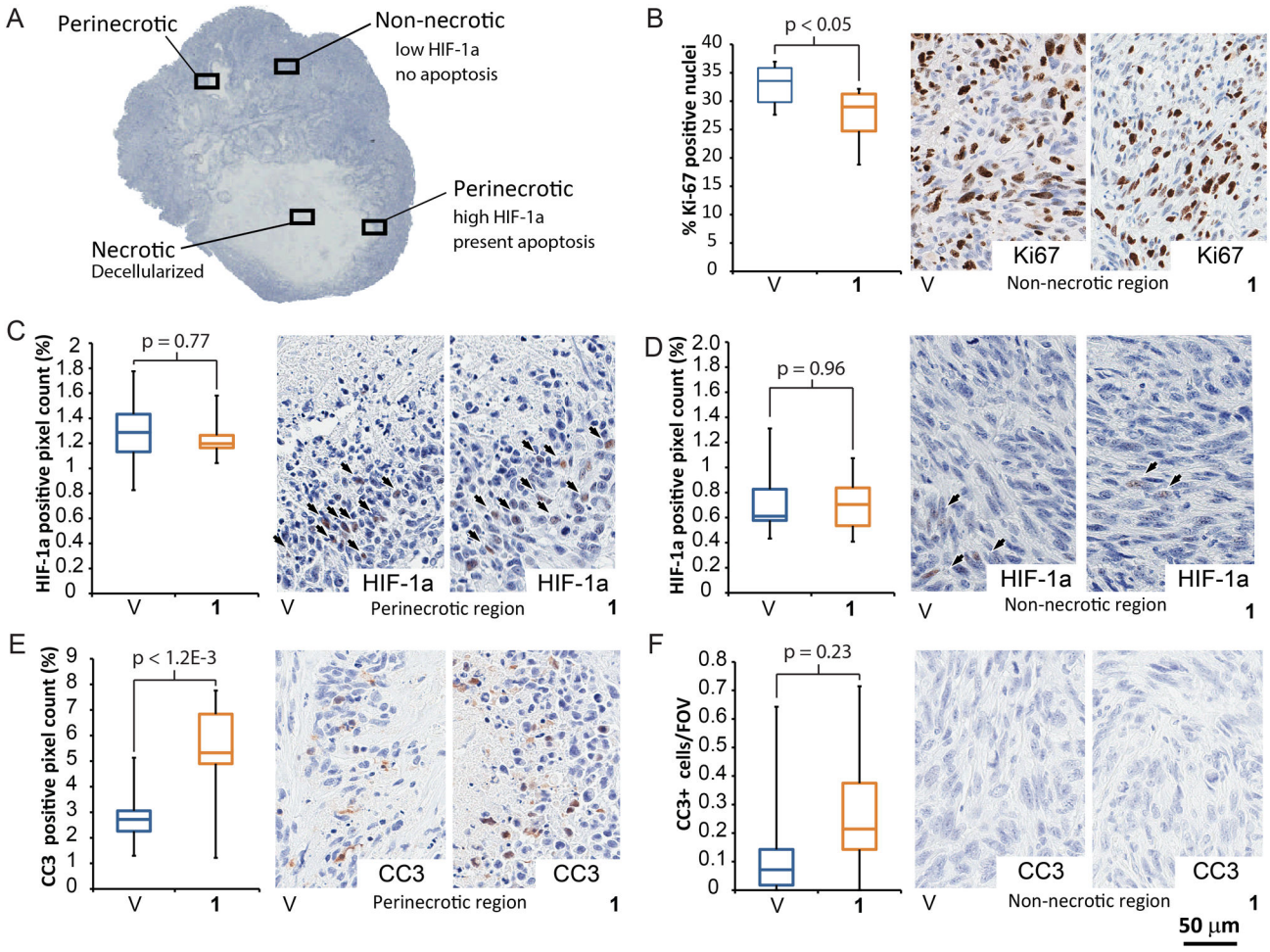

Figure 3. Treatment with 1 decreases tumor proliferation, induces apoptosis in HIF-1a positive areas and does not lead to HIF-1a accumulation

A) Regions used for local analysis in U251 tumors (*Schedule B* treatment). All analysis was done at 20× magnification, perinecrotic area contained 50% necrosis and 50% adjacent, non-necrotic area, as shown. B) Treatment with **1**, induced a modest, but statistically significant decrease in proliferative index (Ki-67 staining). C) The non-necrotic region exhibited low numbers of HIF-1a positive pixels. D) Perinecrotic area was more positive in HIF-1a. However, there were no differences in HIF-1a levels between the treatment groups. E) Cells in perinecrotic region show significant increase in CC3 staining upon treatment with **1.** F) However, non-necrotic tumor regions show no presence of apoptosis. For each measurement n=10, per condition. Error bars denote minimum and maximum.

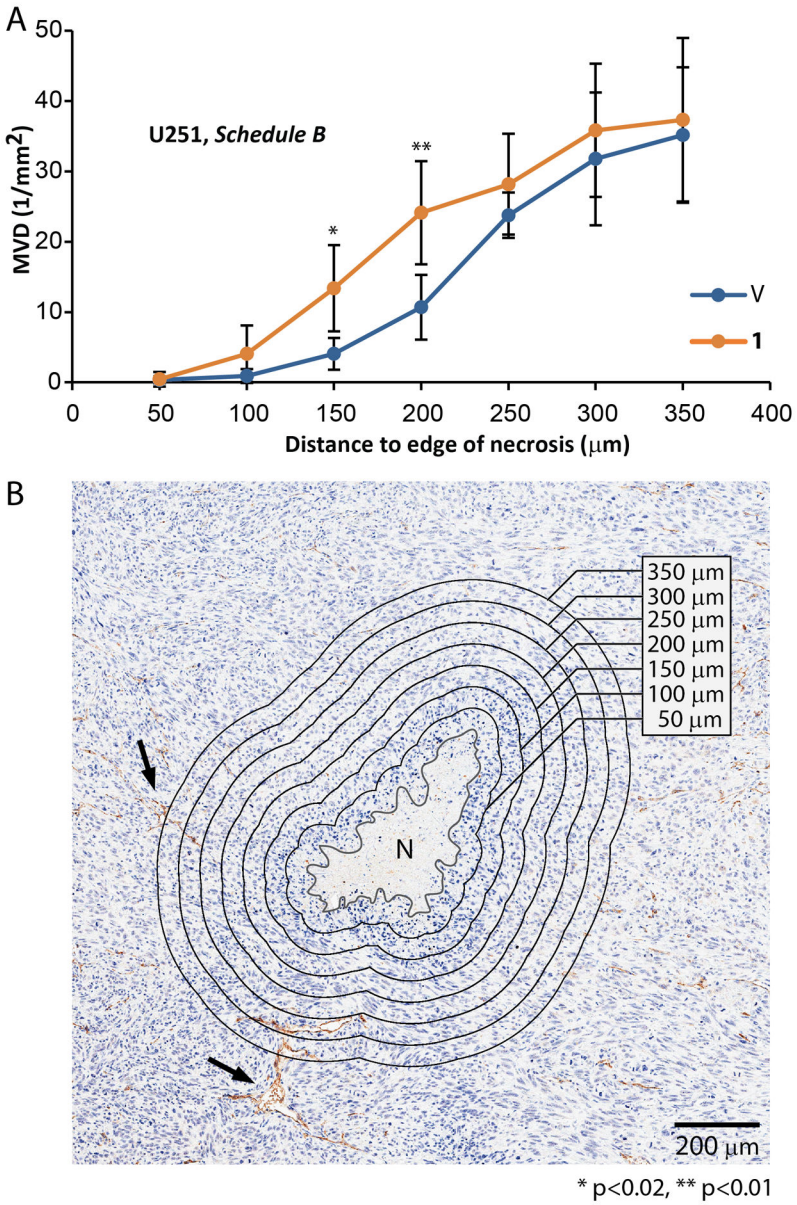

Figure 4. Treatment with 1 increased reliance of tumor cells on proximity to vasculature

U251 cells with impaired adaptation to hypoxia are more sensitive to low oxygen pressures. Necrosis can form in the areas with inadequate oxygen supply, typically at a distance of ~ 200 μm (oxygen diffusion limit in tissue) from blood vessels. As the oxygen pressure is dependent on the blood supply and necrosis is dependent on the oxygen pressure, the density of blood vessels around necrosis is an indirect, phenotypic, endpoint of hypoxic adaptation that is highly quantifiable. To measure the degree of hypoxic adaptation impairment upon the treatment with **1**, necrosis was delineated manually and zones were offset every 50 μm. Number of blood vessels per area was calculated for each zone and converted to MVD. A) Group treated with **1** shows higher MVD in perinecrotic areas - within 150 and 200 μm from the edge of necrosis. B) Example of necrosis along with delineation and zonal analysis of MVD. (n=10 tumor per condition, 854 total microvessels measured for a group treated with

1 and 586 for a group treated with vehicle). Arrows denote two of the large microvessels, N denotes necrosis. Error bars denote 95% CI.

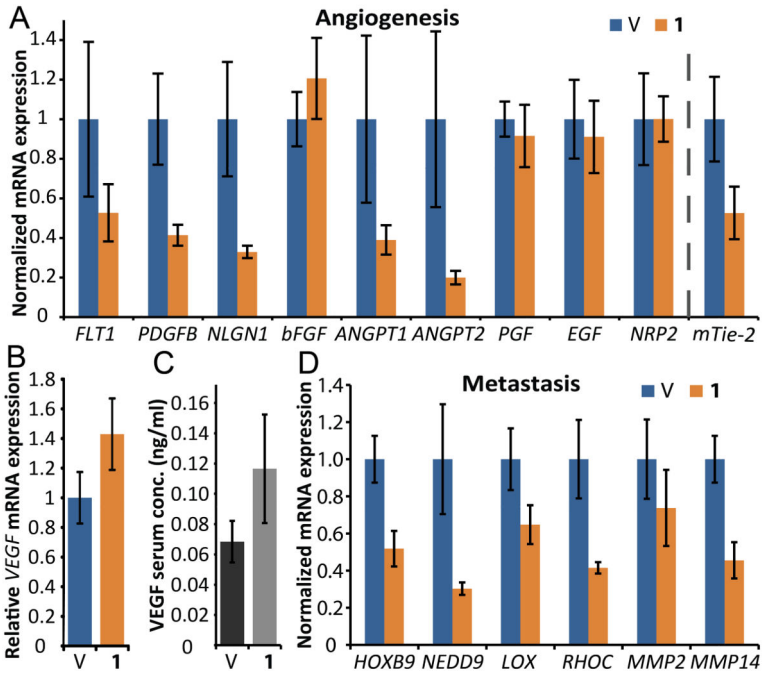

Figure 5. Treatment with 1 inhibits transcription of proangiogenic and prometastatic factors in tumors

Mice harboring U251 tumors were treated according to S*chedule D* to capture gene expression profile underlying the changes in tumor mass and MVD (n=8 per condition). We registered a significant downregulation of several important proangiogenic factors (A), including Angiopoietins 1 and 2 (*ANGPT1, ANGPT2*), overall tumor levels of their receptor mouse-*Tie-2 (Tek)*, Neuroligin 1 (*NLGN1*) as well as Platelet-Derived Growth Factor-B (*PDGFB*). Interestingly, both mRNA expression (B) and serum protein levels of a human-*VEGFA* (C) were upregulated slightly in treated animals (n=8,6 for samples treated with vehicle and **1**). We selected a panel of prometastatic factors and found that **1** inhibits mRNA expression in all tested transcripts except *MMP2* (D). Error bars denote 95% CI.

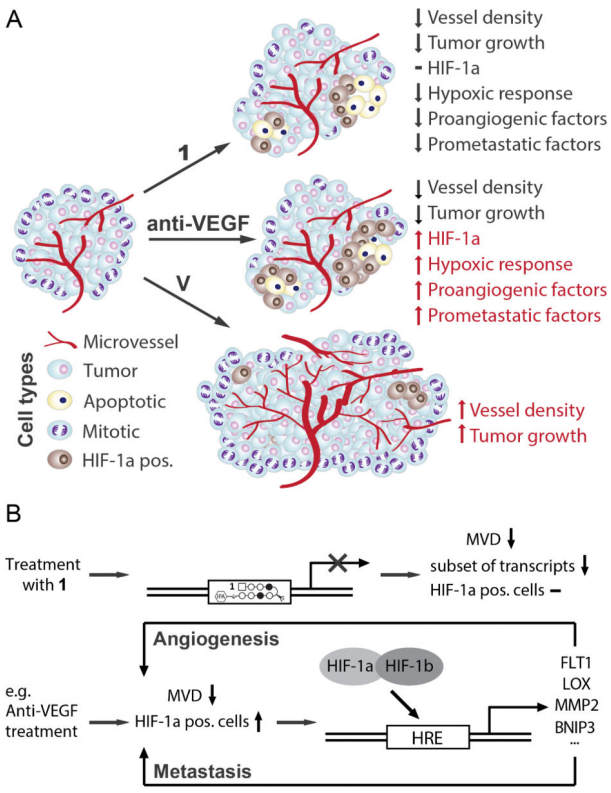

Figure 6. Treatment with 1 inhibits tumor growth and decreases density of vasculature without induction of HIF-1a or expression of proangiogenic factors

A) Compound **1** reduces microvessel density, hypoxia-related gene expression and cell proliferation, but does not increase HIF-1a levels. Presence of apoptosis in HIF-1a positive, but not HIF-1a negative areas, increased reliance of cancer cells on proximity to vasculature also indicate increased sensitivity of cancer cells to hypoxia. B) Therapies targeting angiogenesis that do not impair hypoxic adaptation (e.g. Anti-VEGF) can lead to increased expression of prometastatic and proangiogenic factors. Treatment with **1** inhibits expression of many of those factors, thus contributing to impaired adaptation of tumors to hypoxia.